Available online at www.sciencedirect.com
SCIENCE DIRECT®
Coordination Chemistry Reviews 248 (2004) 1479–1489
COORDINATION CHEMISTRY REVIEWS
www.elsevier.com/locate/ccr

Review

Systematic investigation of the role of compact TiO_2 layer in solid state dye-sensitized TiO_2 solar cells

Bin Peng [a], Gert Jungmann [a], Claus Jäger [b], Dietrich Haarer [b], Hans-Werner Schmidt [a], Mukundan Thelakkat [a,*]

[a] *Macromolecular Chemistry (MCI) and Bayreuther Institut für Makromolekülforschung (BIMF), University of Bayreuth, Universitätsstr. 30, 95440 Bayreuth, Germany*
[b] *Experimental Physics IV (EPIV) and Bayreuther Institut für Makromolekülforschung (BIMF), University of Bayreuth, Universitätsstr. 30, 95440 Bayreuth, Germany*

Received 15 October 2003; accepted 9 February 2004
Available online 24 June 2004

Contents

Abstract 1479
1. Introduction 1480
2. Experimental 1480
 2.1. Materials 1480
 2.2. Instrumentation 1481
 2.3. Solid state dye-sensitized TiO_2 solar cell 1481
  2.3.1. Spray pyrolysis deposition (SPD) of TiO_2 1482
  2.3.2. Screen-printing of nanocrystalline TiO_2 film (nc-TiO_2) 1482
  2.3.3. Coating of the Ru-dye and the hole-transport layer (HTL) 1482
3. Results and discussions 1483
 3.1. Scanning electron microscopic (SEM) studies of the blocking TiO_2 layers 1483
 3.2. Ellipsometric measurements 1484
 3.3. Rectifying behavior of the blocking TiO_2 layer 1485
 3.4. Influence of the blocking layer on the photovoltaic properties 1487
4. Conclusions 1488
Acknowledgements 1489
References 1489

Abstract

The preparation steps of solid state dye-sensitized nanocrystalline TiO_2 solar cells are optimized with respect to the blocking TiO_2 layer which is one of the essential layers in such a multi-layer solar cell. By varying the number of spraying cycles in the preparation of the blocking TiO_2 films, a series of samples with increasing blocking layer thicknesses was prepared. Influence of the layer thickness on the surface morphology was examined using scanning electron microscope (SEM). The thickness and refractive index of the blocking layers were also investigated with ellipsometry measurements. A linear increase in TiO_2 layer thickness with the number of spraying cycles was observed for repetitive spraying cycles between 6 and 30. To characterize the rectifying behavior of the blocking layer, cells with the structure, FTO/blocking TiO_2/hole conductor/Au, were prepared and their current (I)–voltage (V) properties investigated. Solid state solar cells were also prepared with different blocking layer thicknesses and their photovoltaic properties were investigated in order to study the influence of the blocking layer thickness on solar cell performance. From the results, an optimum number of ten spraying cycles (corresponding to a film thickness of 150 nm) for the preparation of blocking TiO_2 is suggested to obtain the best rectifying behavior and best photovoltaic properties

*Corresponding author. Tel.: +49-921-553108; fax: +49-921-553457.
E-mail address: mukundan.thelakkat@uni-bayreuth.de (M. Thelakkat).

0010-8545/$ – see front matter
doi:10.1016/j.ccr.2004.02.008

of the corresponding solar cells. The automated procedure of preparing the blocking layer guarantees reproducibility in obtaining constant thickness and quality of this crucial layer as seen in the current–voltage characteristics of the solar cells.

Keywords: TiO_2 blocking layer; Spray pyrolysis deposition; Solid state dye-sensitized nanocrystalline TiO_2 solar cell

1. Introduction

Dye-sensitized titanium dioxide solar cells employing liquid electrolyte for charge transport as developed by Grätzel and co-workers are still some of the most efficient solar cells outside the realm of inorganic semiconductor cells [1–4]. However, the liquid electrolyte present in such cells creates both short-term and long-term sealing problems and this has activated the search for alternative hole transporting systems such as gelated molten salt electrolytes, polymer electrolytes etc, but still using the inorganic I_3^-/I^- as hole transport medium [5–8]. Major advances were made in this direction. The use of conjugated p-type polymers instead of the electrolyte as charge transport medium was also reported in the literature [9,10]. We have shown that the efficient class of hole transport compounds with a triarylamine structural unit which is well-known for its high hole transport mobility could be used instead of the liquid electrolyte to obtain a solid state dye-sensitized cell [11,12]. This type of solid state cell was later further optimized in the Grätzel group by using a low molecular weight spiro-compound as hole conductor and using additional additives such as lithium salt and dopants to increase the conductivity of such a cell to obtain higher power conversion efficiencies [13,14]. One of the major differences between the electrolyte cell and p-type semiconductor cell lies in the nature of charge transport: ionic transport controlled by diffusion prevails in the former whereas electronic transport influenced by conductivity and charge transport mobility plays the deciding role in the latter.

Moreover, an important difference exists at the interface between the hole transport medium and the transparent working electrode FTO (F-doped SnO_2). In the electrolyte cell, the iodine/iodide has a strong over-potential at this interface, so that a barrier exists to prevent the photo-generated charges from recombination at the boundary. On the other hand, *spiro*-OMeTAD and FTO form an ohmic contact, which means that the charge carriers will recombine at this interface, resulting in an intrinsically inefficient solar cell. One way to solve this problem, which has proven to be difficult [15] is to replace FTO with a material which forms a blocking contact to the hole transport medium. Another approach, as put forward by Grätzel and co-workers, is to put in an additional compact layer of TiO_2 between FTO and nc-TiO_2 layer. Thus, use of an additional blocking TiO_2 layer is essential for the p-type semiconductor cell to avoid short circuiting and loss of current through recombination at the FTO electrode. The fact that the introduction of such a TiO_2 layer between the nanocrystalline TiO_2 layer and the FTO electrode enhances the current output by three to four orders of magnitude clearly points out the importance of this layer.

A compact TiO_2 layer can be prepared by different methods such as electron beam evaporation [16,17], chemical vapor deposition from precursors such as Ti_3O_5 under oxygen partial pressure [18,19] or from other precursors such as tetra isopropyl orthotitanate [20] or by the aerosol pyrolysis deposition [21–23]. Recently, we have demonstrated that chemical vapor deposited TiO_2 layers can be integrated into a fully vapor deposited organic thin layer solar cell in order to improve the charge separation and power conversion efficiency [19]. Kavan and Grätzel [22] have reported in detail the preparation and use of a compact TiO_2 layer obtained by aerosol pyrolysis as photoelectrode in combination with various electrolytes. Recently Grätzel and co-workers have used this type of compact layer efficiently in solid state solar cells [13,14]. The importance of this compact layer is otherwise not yet recognized or exploited by other research groups [24].

This paper describes the details of an automated method of preparation of such a compact layer of TiO_2 by spray pyrolysis of an aerosol of titanium(IV) bis(acetoacetonato) di(isopropanoxylate) (TAA) in ethanol and its standardization for a solid state solar cell containing a p-type organic semiconductor. The nature, structure and morphology of this layer with increasing thickness was examined with scanning electron microscopy (SEM) and the rectifying property of this compact layer was studied by looking into the current (*I*)–voltage (*V*) characteristics of a simplified two-layer diode involving this layer and a hole conductor. Influences of the layer thickness on the photovoltaic properties of the corresponding solar cells were also investigated.

2. Experimental

2.1. Materials

Glass substrates (Type TEC8, 3 mm thick) were purchased from Hartfordglass (Indiana, USA). The substrate, covered with a layer of fluorine-doped tin oxide (FTO) which had a sheet resistance of 8 Ω per square, was cut to a size of 25.4 mm × 25.4 mm and used for the cell preparation. Titanium (IV) bis(acetoacetonato) di(isopropanoxylate) and *N*-lithiotrifluoromethane sulfonimide, $(CF_3SO_2)_2NLi$ (Li-salt), were purchased from Aldrich. TAA was used

as received and Li-salt was dried in vacuum before use. Nanocrystalline titanium dioxide (nc-TiO_2) precursor paste (Ti-oxide TSP) and ruthenium-dye (Ru-535 bisTBA or N719) were bought from Solaronix (Aubonne, Swiss) and used without further treatment. The nc-TiO_2 paste consisted of anatase particles with a diameter of about 13 nm and a surface area of 120 m^2/g according to BET measurement. The paste was diluted in terpineol by the manufacturer to form a pale-yellowish colloidal paste. The dye, *cis*-bis(isothiocyanato)-bis-(2,2′-bipyridyl-4,4′-dicarboxylato)-ruthenium(II)-bis(tetrabutylammonium) has a shortened formula of $RuL_2(NCS)_2(TBA)_2$, where L = 2,2′-bipyridyl-4,4′-dicarboxylic acid and TBA = tetrabutylammonium. A short name, Ru-dye, is used in this paper. 2,2′,7,7′-Tetrakis-(*N*,*N*-di-4-methoxyphenyl amino)-9,9′-*spiro*-bifluorene (*spiro*-OMeTAD) was synthesized according to a procedure known in literature [25]. The *spiro*-OMeTAD radical cation salt (abbreviated as ox.-*spiro*) was obtained by single electron transfer oxidation of *spiro*-OMeTAD with excess of $AgSbF_6$ in toluene. Other solvents and common chemicals were purchased from Aldrich or Fluka and used as received without further purification.

2.2. Instrumentation

The spray pyrolysis deposition (SPD) and screen-printing were carried out using home-made instruments; the details of which are given below. The thicknesses of the blocking layers were measured by field-emission scanning electron microscopy (FE-SEM LEO 1530) and also with spectroscopic ellipsometry (Sentech SE 850). The photovoltaic current–voltage measurements were carried out with a Keithley 6517 Source-Measure unit under AM 1.5 G conditions (Xenon arc lamp, Air Mass Filters from Oriel). The intensity of light was calibrated with a standard Si-reference cell from the Fraunhofer Institut für Solarenergie (ISE), Freiburg as 77 mW/cm^2. Au was deposited by electron beam deposition in a BA 510 vacuum chamber from Balzers (Liechtenstein).

2.3. Solid state dye-sensitized TiO_2 solar cell

Fig. 1 shows schematically the different layers in a solid state Grätzel solar cell modified with an organic hole conductor [13,14]. In this cell, the FTO layer serves as a conducting electrode which is also transparent to let the light through to reach dye-TiO_2 junctions. The next layer, a compact TiO_2 film acts as the blocking layer to prevent holes formed in the dye or HTL layer from reaching the lower FTO layer, which would otherwise short-circuit the cell. The porous structure of the nc-TiO_2 layer enlarges the surface area greatly up to a factor of about 1000 as compared to a flat surface, which enables most of the light to be absorbed, or reflected and then absorbed, resulting in maximum light harvesting. The nc-TiO_2 itself is a network, making it possible for the transferred electrons to reach the anode through this perforated network. A molecular layer of Ru-dye is self-assembled on the nc-TiO_2 surface by chemisorption, forming a heterjunction which functions as an interface for the separation of charges from the excitons formed. The charge separation occurs at the interface, the electron is transferred to TiO_2 and the hole in dye is compensated by electron transfer from HTL (see enlarged part in Fig. 1) [11,13]. The hole-transport layer (HTL) is prepared from a mixture of *spiro*-OMeTAD, radical cation salt of *spiro*-OMeTAD (ox.-*spiro*), and Li-salt. The ox.-*spiro* acts as a dopant to enrich charge concentration and the Li-salt is added to increase conductivity as well as to manipulate the surface potential of TiO_2 to enhance electron injection.

As shown in Fig. 2, we typically prepared four cells on a substrate to check the reproducibility. The different layers are deposited in the middle (area b3) of the substrate followed by the deposition of a layer of gold on areas b1

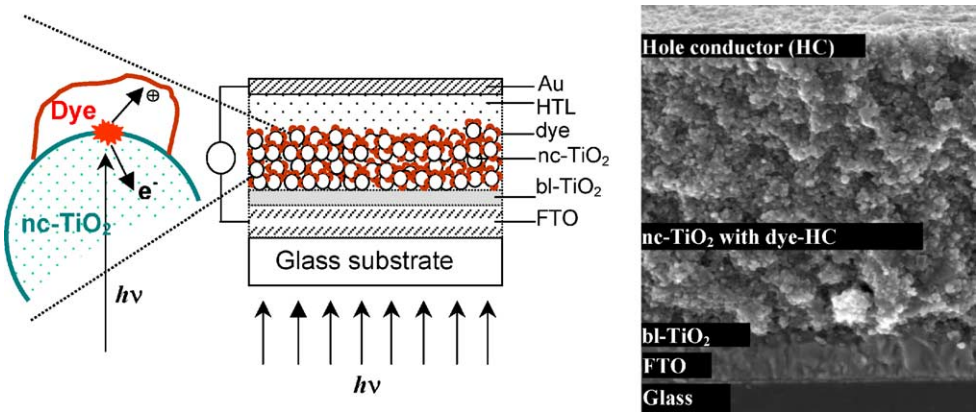

Fig. 1. A schematic description and SEM cross-section of the different layers in a solid state, dye-sensitized nanocrystalline TiO_2 solar cell. A fluorine-doped tin oxide (FTO) layer forms the transparent anode. The blocking TiO_2 layer (bl-TiO_2) is to avoid the recombination and short circuiting at the FTO anode. The nanocrystalline TiO_2 (nc-TiO_2) provides large surface area on which a mono-molecular layer of the Ru-dye is chemisorbed and this forms a heterjunction where light-harvesting and charge separation take place. The separated electrons and holes are conducted through TiO_2 to the FTO-anode and through the organic hole-transport layer (HTL) to the Au-cathode, respectively.

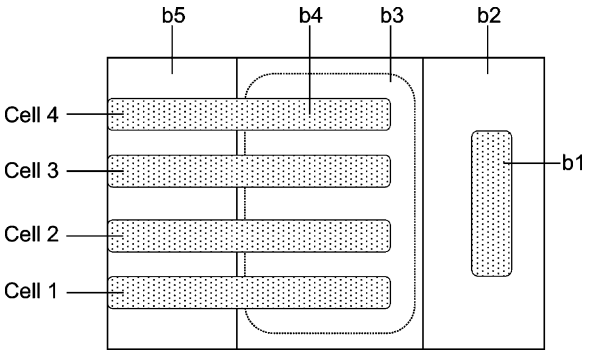

Fig. 2. The solar cell structure with four identical cells showing the different contacts and regions on a glass substrate (25.4 mm × 25.4 mm). The different layers are deposited in the middle (area b3) followed by the deposition of a layer of gold on areas b1 and b4 (shaded regions). FTO on area b5 was etched away, whereas on area b2 there is bare FTO. Effective area of each cell is the common region of areas b3 and b4, which is 8 mm × 2 mm (0.16 cm^2).

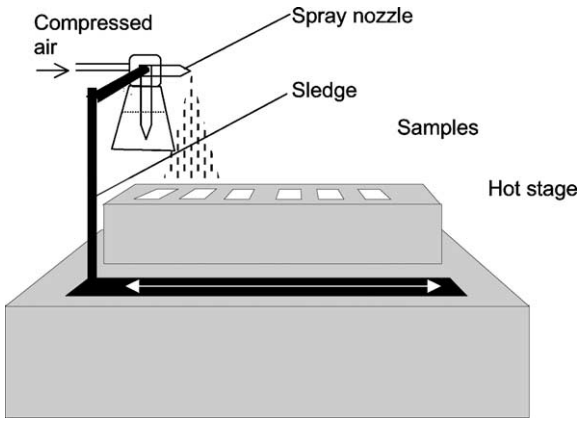

Fig. 3. Schematic setup for automated spraying pyrolysis deposition (SPD). Temperature of the hot stage and moving speed of the sledge are controlled by regulators. Number of spraying cycles and intervals between two cycles are adjustable. In a SPD process, an aerosol of titanium(IV) bis(acetoacetonato) di(isopropanoxylate) (TAA) is created and sprayed on to the substrate kept at a temperature high enough to burn off all the organics, thus leaving behind a compact layer of TiO_2.

and b4 (shaded regions). FTO on area b5 was etched away with zinc powder and HCl, whereas on area b2 there is bare FTO, i.e., without any layers except Au deposition on b1. The effective area of each cell is the common region of areas b3 and b4, which is 8 mm × 2 mm (0.16 cm^2), where the photo-induced charges are collected to the outer circle. Solar cell samples were prepared by successive deposition of the component layers as follows. First a compact layer of bl-TiO_2 was deposited via SPD followed by a nc-TiO_2 film by screen-printing. After sintering the nc-TiO_2, the substrate was immersed in a Ru-dye solution for dye-coating. Physisorbed dye molecules were subsequently washed away and a HTL layer was spin-coated as the next step. Finally, with a mask, a thin Au-film was vapor-deposited. The next sections give a detailed description of layer-by-layer preparations of a solar cell.

2.3.1. Spray pyrolysis deposition (SPD) of TiO_2

The TiO_2 blocking layer (bl-TiO_2) was prepared by spray pyrolysis deposition [22,23]. An SPD setup was developed in our lab, and the spraying procedure was automated to avoid errors by manual work. Fig. 3 sketches the principles and the components of the SPD setup. The setup consisted mainly of a hot-plate whose temperature could be controlled, a reservoir with a nozzle and a sledge which moved the sprayer. A programmable controller connected to the sledge could regulate the moving speed of the sprayer, the number of spraying cycles and the interval between the spraying cycles.

To carry out the SPD, cleaned FTO glass substrates were put on the hot plate and heated to 450 °C. By blowing compressed air in a perpendicular direction to the suction capillary tube in the vicinity of its opening in the nozzle, the solution containing TiO_2 precursor in the reservoir was sucked by and mixed with the air and the aerosol formed was driven to the heated substrate by the blowing force of the compressed air. The temperature of the hot plate was high enough to pyrolyze any organic substance to gases, leaving behind titanium dioxide to form a compact film on the substrate.

The preparation conditions of the TiO_2 blocking layer with the SPD setup were systematically optimized in our lab to obtain reproducible and smooth films. The organo-titanium compound, TAA, diluted with ethanol to a concentration of 0.2 M was used as the spraying solution [22]. The pyrolysis was carried out at 480 °C. After the required number of spraying cycles under optimized conditions, the substrates ware annealed at 500 °C for another hour before cooling down to room temperature. The substrates were kept in an inert atmosphere for further layer preparation.

2.3.2. Screen-printing of nanocrystalline TiO_2 film (nc-TiO_2)

Nanocrystalline TiO_2 was deposited on the compact TiO_2 layer by screen-printing. A substrate with bl-TiO_2 was fixed on the screen-printing setup by vacuum chuck and nc-TiO_2 paste was swept over a sieve (mesh size 173 μm) with a plastic block. After removing the sieve, a film of nc-TiO_2 paste was left behind on the substrate. The sample was subsequently sintered, first at room temperature for half an hour to evaporate organic solvents, followed by heating to 500 °C at a heating rate of 4 °C/min and kept at 500 °C for another 30 min before being cooled down in ca. 1.5 h to about 80 °C for dye coating. The nc-TiO_2 layer thickness after sintering was around 3 μm.

2.3.3. Coating of the Ru-dye and the hole-transport layer (HTL)

Ru-dye was dissolved in a mixture of acetonitrile and *tert*-butanol (volume ratio 1:1), forming a 0.5 mM dark reddish-brown solution which was filtered through a 1 μm filter (Whatmann, Ann Arbor, MI). Water-free sol-

vents were used and the preparation was carried out at room temperature in a flow box under continuous flux of an inert gas, which keeps the box relative humidity at about 30%.

After being cooled down to about 80 °C from the sintering step, the substrates were transported directly into the dye solution. The nc-TiO_2 is made up of very small particles and, therefore, plenty of minute holes and cavities exist in the film. The "warm-condition" of the sample (80 °C) prevented moisture from being absorbed in the cavities, which can otherwise reduce the surface area available for active self-assembly of the Ru-dye molecules. Dye coating was carried out at room temperature in the flow box in the dark for 18–20 h. Thereafter, the physisorbed dye molecules were rinsed away by dipping the samples in dry ethanol for 1 h. The samples were subsequently dried in vacuum at 45 °C for at least 3 h.

The hole-transport layer was spin-coated as the next step. *Spiro*-OMeTAD (0.16 M), and ox.-*spiro* (0.16 mM) were dissolved in water-free chlorobenzene, and Li-salt (15 mM) in cyclohexanone. (Other solvent combinations were tested for the Li-salt, but the quality of the resulting HTL films was very poor.) From the above solutions, 7.2 volume portions of *spiro*-OMeTAD, 1.8 portions of ox.-*spiro*, and one portion of Li-salt solutions were mixed and filtered through a 0.25 μm Teflon filter (Whatmann). For each substrate, 150–200 μl of the hole-conductor solution was used for the spin-coating.

After spin-coating, the hole-conductor materials on both edges of the substrate (areas b2 and b5 in Fig. 2) were removed by rubbing softly with cotton swabs wetted with toluene. The substrates were then dried in vacuum at 45 °C over night. As the final step, 200 nm Au-layer was vapor-deposited with the help of a mask (cf. Fig. 2).

3. Results and discussions

By varying the number of spraying cycles in the preparation of the blocking TiO_2 films, a series of samples with increasing blocking layer thickness (spraying cycles: 1, 2, 3, 4, 6, 8, 10, 12, 14, 16, 18, 22, 26, 30) on top of FTO-coated glass substrate was prepared. The influence of the increasing bl-TiO_2 thickness on the surface morphology and the film thickness was examined by scanning electron microscopy. The refractive index and thickness were further measured with ellipsometry [26]. To characterize the rectifying effects of the bl-TiO_2, current–voltage properties of cells with the structure, FTO/bl-TiO_2/HTL/Au, with different bl-TiO_2 layer thickness were investigated. Moreover, solar cells were also prepared with the structure, FTO/bl-TiO_2/nc-TiO_2/Ru-dye/HTL/Au, in which only bl-TiO_2 layer thickness was varied and their photovoltaic properties investigated to study the influence of the blocking layer thickness.

3.1. Scanning electron microscopic (SEM) studies of the blocking TiO_2 layers

Fig. 4 shows the SEM pictures of top-view (a, c, e) and cross-section (b, d, f) of bare FTO and compact titanium dioxide films with 8 and 30 spraying cycles, respectively. The cross-section images were taken at a 5° tilted angle, making it possible to have a roughly lateral look on the sample surface. The magnification factor of these pictures in Fig. 4 is 50,000×. The bare FTO surface shows characteristic morphology of tin oxide crystals (Fig. 4a). The corresponding cross-section picture (Fig. 4b) reveals a thickness of ca. 500 nm for the FTO with a uniform and homogenous relief. Fig. 4c displays a surface after eight cycles of TiO_2 spraying deposition. Most of the small FTO particles were covered by the TiO_2, and the sharp edges of bigger FTO particles were rounded off by the deposition. Apparently, TiO_2 was growing on top of the FTO particles, taking up the structure of the underneath surface relief. This point is further supported by observing the side-view picture (Fig. 4d) where it can be seen that the TiO_2 surface morphology is "smoothed" to some extent, but predominantly maintaining the underneath FTO relief morphology.

The particle-like pattern seen in Fig. 4c is, therefore, the result of the deposition, layer upon layer, of TiO_2 on the FTO particles, the relief of the latter determining the morphology of the above-grown TiO_2. This notion is somewhat different from the one proposed by Kavan and Grätzel [22], who have observed that TiO_2 "particles" grow on the top of FTO surface. From the SEM pictures they have measured the particles size of a 100 nm thick TiO_2 film to be in the range of 49–56 nm. Interestingly, structures of similar size range were also noticed with a TiO_2 film which had a thickness of 125 nm (Fig. 4c, see below). As discussed above, however, the seemingly particle-like patterns of TiO_2 were the result of the growth of TiO_2 on top of the FTO morphology lying underneath.

A different morphology of the FTO would have resulted in a different TiO_2 pattern. The cross-section picture displays a compact, crack-free TiO_2 film which is dense and continuous (the 10 nm sized sub-structures arise due to a 3 nm Pt layer deposited to increase the conductivity of the surface in the SEM analysis). The thickness of the bl-TiO_2 film determined with the SEM, is 122 ± 5 nm for eight spraying cycles.

After 30 TiO_2 spray deposition cycles (Fig. 4e), the sharp edges and the smaller particle structure are almost completely disappeared as a result of the repeated efficient compact layer formation. Only big particles with gentle edge-curves are to be seen (Fig. 4e). While shapes and similarities in size distributions between the underneath FTO particles and the TiO_2 pattern on the surface can still be slightly recognized after eight cycles of TiO_2 spraying (compare Fig. 4a and c), there is hardly any resemblance either in the appearance or in the size distribution to be identified after 30 deposition cycles (compare Fig. 4a

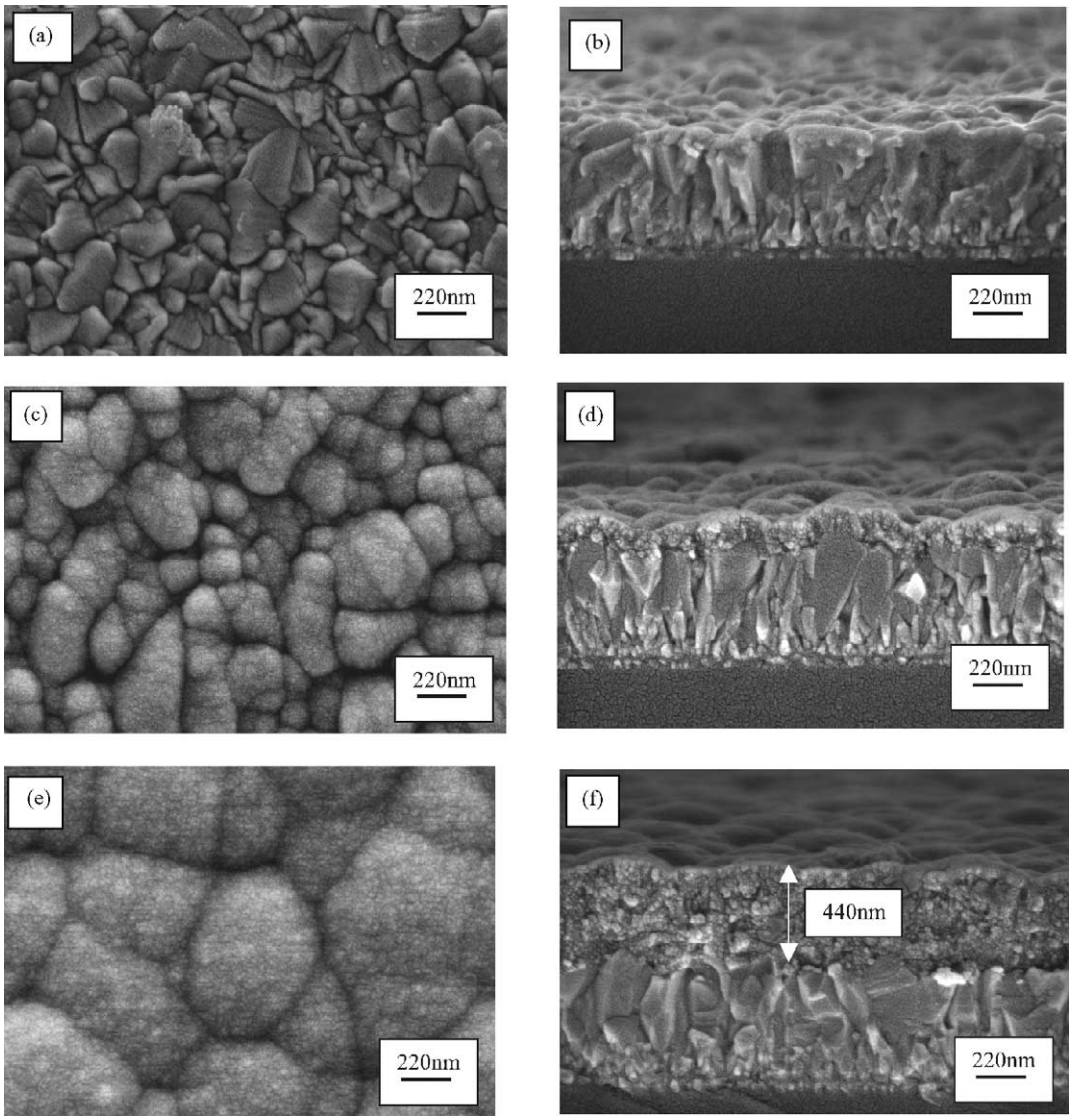

Fig. 4. Scanning electron microscope (SEM) pictures of bl-TiO_2 layers prepared by eight spraying cycles (c, surface and d, cross-section) and 30 spraying cycles (e, surface and f, cross-section) compared with bare FTO layer (a, surface and b, cross-section). Thickness of the TiO_2 layer in (d) and (f) are 120 and 440 nm, respectively.

and e). A lateral view of the 30-cycle sample reveals quite a smooth surface with very gentle roughness, with hardly any trace of the surface morphology of the starting FTO being preserved. The thickness of the TiO_2 layer obtained after 30 spraying cycles was determined to be 440 nm (Fig. 4f). This suggests roughly a thickness of about 15 nm per spray deposition cycle for TiO_2.

We obtained thicker TiO_2 films than those of Kavan et al. [22], who have got a film thickness of 80–100 nm after 20 repetitive spraying cycles with the same concentration of spraying solution. This might have arisen from the differences in the preparation conditions, which are very difficult to be controlled and reproduced if done in a manual way. Parameters such as the air pressure, the spraying rate, distance between the nozzle and the substrates can all affect thickness of the resulting TiO_2 films. The automated procedure presented here avoids uncertainties in the reproducibility of these films.

3.2. Ellipsometric measurements

Ellipsometry is a fast, precise and non-destructive measurement tool to determine the refractive index (n) or the thickness (d) of a sample [26]. Unfortunately the two parameters are not independent of each other and therefore, they cannot be determined in absolute terms in just one experiment. Extra information about n or d should be obtained beforehand by other techniques. In our investigation, the thickness of two bl-TiO_2 samples could be acquired by SEM (see Section 3.1) which was used for the spectroscopic ellipsometric fittings to get the refractive index of these TiO_2 layers. This n value is then used for thick-

ness determination of further bl-TiO_2 samples. Using the same samples, ellipsometry was carried out before carrying out the SEM, for the samples had to be cut into pieces and evaporated with platinum. With the Sentech 850 ellipsometer, multiple angle measurements were carried out for angles of incidence of 50°, 55° and 60° to obtain the wavelength dependent delta and the psi values, which describe the phase shift and the ellipticity of the reflected light beam, respectively. No retarder was used and the data were analyzed with an implemented fitting routine using a Cauchy layer as model system using the following formulae [27]:

$$n(\lambda) = n_0 + c_0\frac{n_1}{\lambda^2} + c_1\frac{n_2}{n^4} \quad \text{and}$$

$$k(\lambda) = k_0 + c_0\frac{k_1}{\lambda^2} + c_1\frac{k_2}{n^4}$$

where $c_0 = 10^2$, $c_1 = 10^7$, λ is the wavelength, and n_0, n_1, n_2, k_0, k_1 and k_2 the fitting parameters.

Due to the fact that thinner TiO_2 layers cause only few interference peaks, the simulation becomes more and more difficult for thinner layers. Therefore, the thickness value of the thickest sample (440 nm) from the SEM investigation was used as starting parameter to obtain the refractive index. A simultaneous fit (fitting routine SpectraRay by Sentech Instruments GmbH) of all six data sets (psi and delta) was carried out and within the errors the simulation was matched well to the measured curves assuming a 2 nm thickness variation over 1 mm of the TiO_2 layer. Thus, a refractive index of 2.59 at a wavelength of 632.8 nm for the 440 nm thick sample could be determined (Parameters for the relation: $n_0 = 2.594$, $n_1 = -244.7$, $n_2 = 104.4$, $k_0 = -0.033$, $k_1 = 326.486$, $k_2 = -249.605$). Assuming that the refractive index is constant for different layer thicknesses of TiO_2, it was possible to determine the different thicknesses for the other thinner samples as well by changing the thickness parameter. The shape and number of the peaks of interference pattern of the delta and psi data sets could be nicely reproduced by the simulations. It was also possible to reproduce the thickness measurement of a thinner sample which was also determined by SEM for eight spraying cycles: (in SEM, $d = 122\,\text{nm} \pm 5\,\text{nm}$ and in Ellipsometry, $d = 126\,\text{nm}$). The assumption that the refractive index of the TiO_2 layer is independent of the thickness seems to be correct and so it is possible to use one set of parameters of an ellipsometric measurement of a thick sample to determine the thickness of thinner samples. On plotting the thickness obtained by SEM and ellipsometric measurements against the number of spray cycles we note that the thickness of the compact layers is reasonably proportional to the number of spraying cycles above six (see Fig. 5). The dashed line represents a linear fit of the thickness measured by ellipsometry. These results suggest that one spraying cycle leads to about a 15 nm thick TiO_2 compact layer.

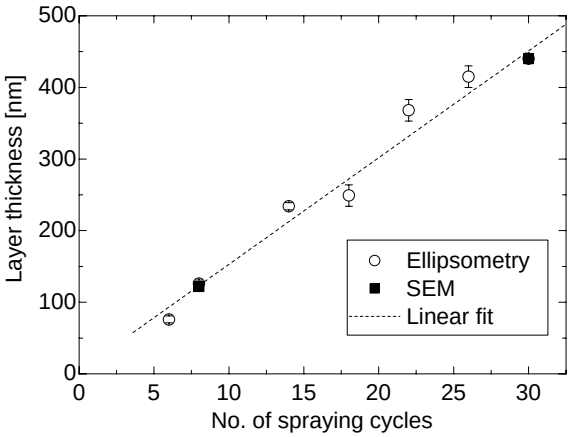

Fig. 5. Thickness of bl-TiO_2 layers obtained from ellipsometry measurements as a function of the number of spraying cycles. The thickness data obtained from SEM (dark squares) agree with the ellipsometric data (thicknesses for less than six spraying cycles show uncertainties in the ellipsometric method and therefore are not taken account of, in this plot) and the thickness is seen to vary proportional to number of spraying cycles.

3.3. Rectifying behavior of the blocking TiO_2 layer

The energetics at the interfaces and the function of a blocking TiO_2 layer can be better understood by looking into the energy level diagram as given in Fig. 6. In an ideal case, the separated electrons from the exciton produced in the dye should flow out through the TiO_2 to the FTO electrode and the hole produced in dye should be compensated by electrons flowing from the Au electrode through the hole conductor to the dye. Any backward flow of electron from FTO to the dye or HTL layer results in recombination of separated charges which worsens the performance of the

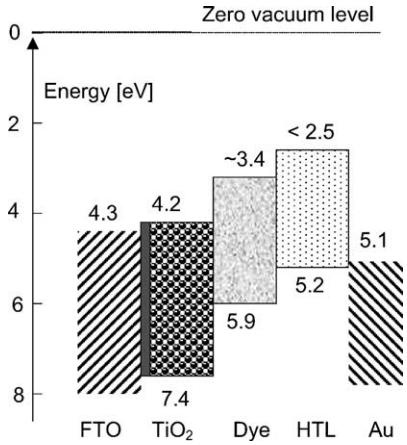

Fig. 6. Energy level diagram showing the work functions and HOMO/LUMO energy values of the respective materials constituting the different layers in the solid state dye-sensitized TiO_2 solar cell. The values given correspond to solid state values. For the dye and HTL, cyclic voltammetry measurements in solution gave the HOMO energy value as 5.6 and 4.9 eV, respectively, which are corrected by including the polarization energy factor of 0.3 eV [28] to obtain 5.9 and 5.2 eV, respectively, in solid state.

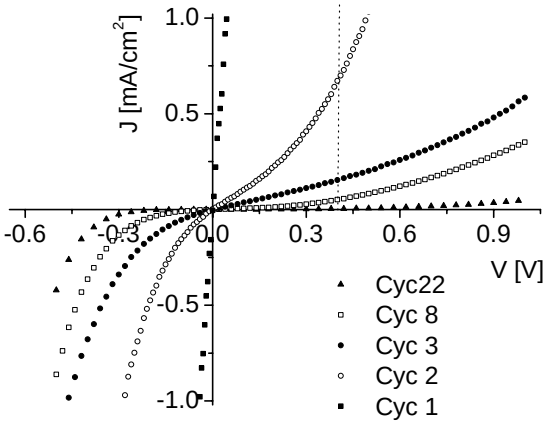

Fig. 7. Current–voltage curves showing increasing rectifying behavior of the blocking layers for increased number of spraying cycles or increasing thickness of bl-TiO_2 layer for cells, FTO/bl-TiO_2/HTL/Au where"/'' stands for a interface, and HTL consists of *spiro*-OMeTAD and ox.-*spiro*. For the purpose of clarity, only five different thicknesses are shown here.

solar cell. The important function of the TiO_2 blocking layer is to block the passage of electrons from FTO to the HTL (or in other words to block the passage of holes from HTL to the FTO) and this can be studied by examining the rectifying behavior of such a bl-TiO_2 layer. For this purpose, we have built simple cells with a blocking TiO_2 layer and a hole-transporting layer between the FTO and Au electrodes, omitting the nanocrystalline TiO_2 film and the dye and *I–V* properties were studied for different bl-TiO_2 thicknesses for the cell-type: FTO/bl-TiO_2/HTL/Au, where"/'' represents the interface between two layers, and HTL consists of only *spiro*-OMeTAD and ox.-*spiro* (i.e., without Li-salt). The voltage was increased continuously from -0.5 to $+1.0$ V with FTO biased negative and Fig. 7 displays the *I–V* curves measured in the dark for samples with different bl-TiO_2 thicknesses. In case of no bl-TiO_2 layer, no Schottky contact was formed and a linear *I–V* relationship was obtained according to the Ohm's Law (curves are not shown here). The device with one spraying cycle bl-TiO_2 layer exhibits also a linear current–voltage relationship, revealing that there was no rectifying behavior and no continuous film was formed.

After two cycles of TiO_2 deposition, the *I–V* curve of the resulting device takes the form of an anti-S shape. This type of behavior points to the existence of typically many small pinholes in thin films. From the third spraying cycle on, the cells show a blocking effect of the TiO_2 layer, illustrating the presence of continuous, pinhole-free, compact TiO_2 films. These results suggest that upon spray pyrolysis deposition the TiO_2 films grow as follows: first, non-continuous, isolated TiO_2 spots are formed; then a continuous layer takes form with pinholes existing therein and from the third spraying cycle onwards, the film becomes continuous, pinhole-free and compact.

It can be seen in Fig. 7 that with increased bl-TiO_2 thickness, less current density (in the first quadrant) and higher breakthrough voltage (in the third quadrant) were measured. For cells with very thick bl-TiO_2 (30-cycle deposition or TiO_2 thickness ca. 450 nm), the current densities in both negative and positive voltage regions were very small and was in the range of several $\mu A/cm^2$. The current density values from the *I–V* curves in Fig. 7 give us very important information about the rectification ability of the bl-TiO_2 films. More current density in the first quadrant means that more electrons are injected from FTO through the bl-TiO_2 into HTL or holes from HTL have passed through the blocking film and reached the FTO-anode, which indirectly implies recombination of charges produced later in a solar cell under this bias conditions of measurement. Thicker bl-TiO_2 films can prohibit this loss, i.e., thicker bl-TiO_2 film can better block the holes produced from getting through to the anode and, therefore, result in a better overall performance of the cell. Thicker compact bl-TiO_2 can, on the other hand, also hinder the desired transport of electrons from reaching the FTO-anode due to inclusion of traps and impurities, which will therefore reduce the performance in a solar cell. For the overall performance of a solar cell, there exists an optimum thickness or thickness region for the blocking TiO_2 layer, in which there is a balance of rectifying property and electron transport.

The rectification ratios (the ratio between current at forward bias to current at backward bias) at a bias of 0.4 V ($V = 0.4$ V is the typical open-circuit voltage, V_{OC}, for the solar cells investigated in this study, see Fig. 10) for samples with two and three spraying cycles are almost negligible. The ratios of samples with 8 and 22 spraying cycles are 14 and 3.3×10^2, respectively. To understand this better, we can draw a perpendicular line at a definite voltage, say, at $V = 0.4$ V (the dotted line in Fig. 7), the intersections of this line with the *I–V* curves for different bl-TiO_2 layer thickness give the current density that passes through the bl-TiO_2 when the voltage ($V = 0.4$ V) is applied to the sample. It is clearly seen that even for eight spraying cycles, the current loss is about 10% at $V = 0.4$ V for a cell delivering an I_{SC} of 1 mA/cm^2.

To make it more understandable, in Fig. 8 the current flow in the first quadrant for two different typical voltages of 0.4 and 0.8 V are plotted as a function of the number of spraying cycles ($V = 0.8$ V is the V_{OC} of a modified Grätzel solar cell with special additives and improved properties reported in the literature [14]).

Typically, the short-circuit current, I_{SC}, in our case is around 1 mA/cm^2 (see also Fig. 10). If we allow the current loss due to recombination at FTO to be, say, 0.1 mA/cm^2 (i.e., 10% with respect to I_{SC}) at an applied voltage of 0.4 V (see horizontal line which passes through $I = 0.1$ mA/cm^2 in Fig. 8), then more than four spraying cycles (or a thickness of more than 60 nm) are necessary for the bl-TiO_2 to meet this requirement. In a similar way, for a 1% (of I_{SC}) of current flow (0.01 mA/cm^2, the dash-dot line in Fig. 8) for the same voltage, $V = 0.4$ V, it requires a minimum number of 14 spraying cycles, or a blocking TiO_2 thickness of at least 200 nm. For cells with open-circuit voltage $V_{OC} = 0.8$ V, even thicker bl-TiO_2 films are needed to meet

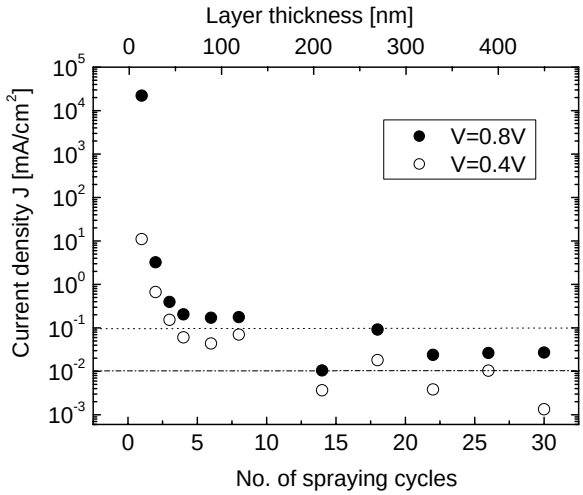

Fig. 8. Influence of the blocking layer thickness (bl-TiO_2 layers prepared by varying the number of spraying cycles from 1 to 30) on the rectifying behavior for devices FTO/bl-TiO_2/HTL/Au at selected voltages of 0.4 and 0.8 V.

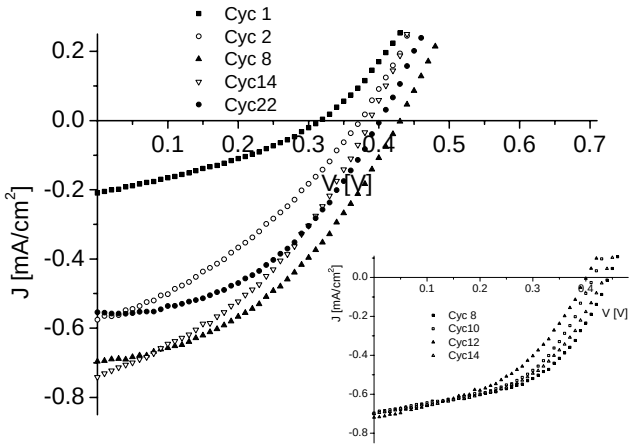

Fig. 9. Current–voltage characteristics of the solid state solar cells for different thicknesses of bl-TiO_2 layers (for clarity, only data for spraying cycles 1, 2, 8, 14 and 22 are shown). The inset shows the constant behavior of cells having bl-TiO_2 layer thickness between 120 and 200 nm (corresponding to 8 and 14 cycles of SPD) which is the optimum region of thickness for best solar cell performance.

the same blocking effect. The quintessence of this study is that for appreciably high open-circuit voltage, a thickness of about 150 nm of bl-TiO_2 is necessary to have the required blocking effect to minimize the current loss due to recombination at FTO electrode.

3.4. Influence of the blocking layer on the photovoltaic properties

A solid state, dye-sensitized nanocrystalline TiO_2 solar cell can be represented by the following formula: FTO/bl-TiO_2/nc-TiO_2/Ru-dye/HTL/Au, where "/" stands for the interface, and HTL consists of *spiro*-OMeTAD, ox.-*spiro* and Li-salt. To study the influence of the blocking layer and its thickness on cell performance, a series of solar cells was prepared with the blocking layer thickness as the only variable parameter (deposition of TiO_2 from 0 to 30 cycles) and all other parameters being kept constant.

For the purpose of clarity, *I–V* curves of only some selected solar cells with 1, 2, 8, 14, and 22 spraying cycles are shown in Fig. 9. The solar cell without bl-TiO_2 exhibited an almost linear *I–V* curve (not shown) whose I_{SC} is below 10^{-7} A/cm^2, and V_{OC} less than 1 mV. Evidently, the cell had short-circuited and scarcely any output power could be obtained from such a solar cell. The very poor performance of solar cells without the blocking layer prove the need for this layer as an indispensable component in solid state dye-sensitized solar cells.

Even though no proper uniform film was formed upon one cycle of TiO_2 deposition, the corresponding solar cell exhibited, as compared with the cell without bl-TiO_2, a considerably improved performance with $I_{SC} = 0.2$ mA/cm^2 and $V_{OC} = 310$ mV (solid square in Fig. 9). The reason is that, although the film was not continuous, as discussed above, there were places where bl-TiO_2 existed as patches which functioned as the blocking layer and contributed to the resulting performance, due to partial suppression of recombination at FTO.

The cell with two deposition cycles exhibited much better performance. The TiO_2 film, though containing pinholes, was much more continuous than that from one deposition cycle and acted more effectively as a blocking layer and therefore much better performance was, therefore, obtained as expected. The huge loss in current density (ca. 0.7 mA/cm^2, see Fig. 7) due to the unsatisfactory rectifying behavior of the bl-TiO_2 here clearly explains the reduced I_{SC} of this cell as compared to that of the best performance cells. The rectifying behavior shown in Fig. 8 exhibits similar results, that is, the current flow decreases very rapidly for devices with spraying cycle 0 to cycle 2 and from cycle 3 onwards the decreasing tendency becomes much more gentle.

A kind of plateau in the performance is observed for cells which had bl-TiO_2 layers from deposition cycles 8–14 (see inset in Figs. 9 and 10). The thickness of the bl-TiO_2 was accordingly 120–200 nm. We can, therefore, suggest that a continuous, compact, pinhole-free TiO_2 layer is the prerequisite for an efficient blocking layer, and this is guaranteed in the thickness range of 120–200 nm. In this thickness range, good rectifying behavior was observed and the overall performance of the corresponding solar cells remains almost constant. This can be seen in the constant and comparable performance of the cells shown as inset in Fig. 9.

An additional increase in the bl-TiO_2 thickness above 200 nm resulted in a worsening of the performance of the corresponding solar cells (Figs. 9 and 10). The cell with 22 spraying cycles (bl-TiO_2 thickness ca. 330 nm) showed more than 30% decrease in the I_{SC} and the cell with 30 spraying cycles (bl-TiO_2 thickness ca. 450 nm) even more than 50%. Thus, a thick bl-TiO_2 can block the holes very

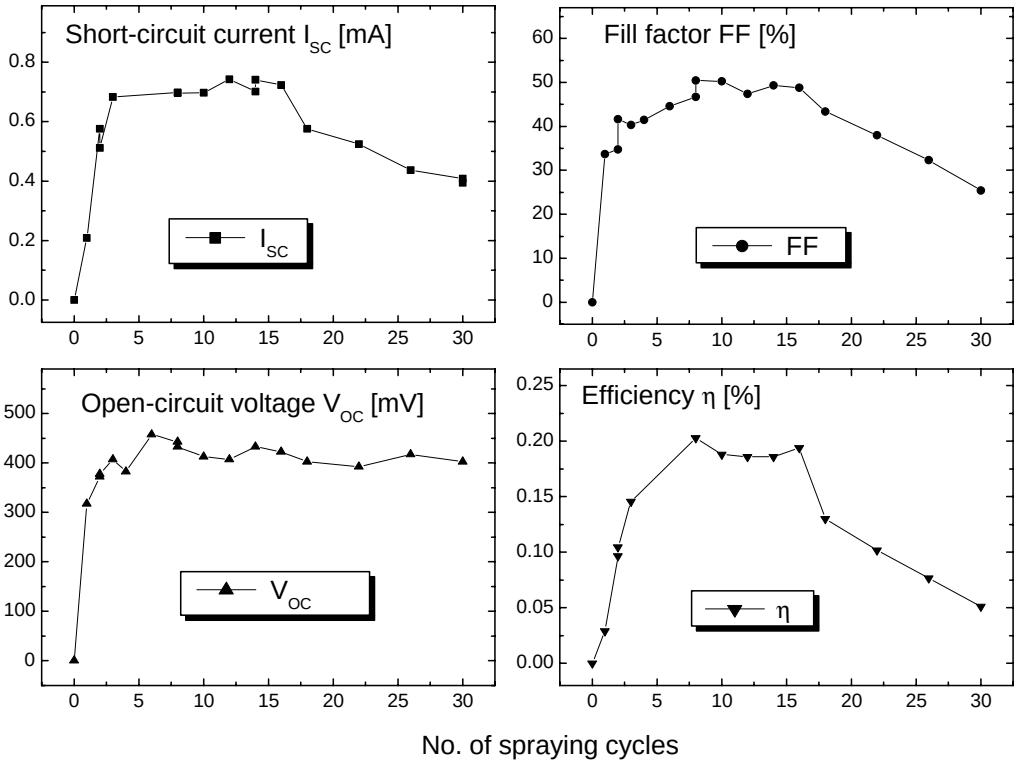

Fig. 10. Influence of the blocking layer thickness obtained by different number of cycles of SPD on the photovoltaic parameters (short-circuit current, I_{SC}; open-circuit voltage, V_{OC}; fill factor, FF; and efficiency η).

efficiently, which is advantageous for the solar cell performances; but when TiO_2 is too thick, this very layer will, on the other hand, hinder electrons from reaching the anode, which worsens the performance of solar cells.

The resulting cell performance in terms of I_{SC}, V_{OC}, fill factor (FF) and power conversion efficiency (η) are plotted in Fig. 10 for all the different thicknesses of bl-TiO_2 layer obtained by different number of spraying cycles. The short-circuit current, I_{SC}, shows a maximum-plateau between Cyc-5 and Cyc-14 (Cyc for cycle). For the fill factor curve there is a wider maximum-region which covers the region from Cyc-4 to Cyc-22. A saturation effect can be observed in the open-circuit voltage, V_{OC}, curve. The V_{OC} reached 400 mV at Cyc-4 and stayed around this value for all the thicker bl-TiO_2 cells. The efficiency, η, is defined by the equation,

$$\eta = \frac{I_{SC} V_{OC} FF}{P_{input}}$$

where P_{input} is the input power which was the same for all the measurements. Thus, η reflects the resulting product of the three parameters, I_{SC}, V_{OC} and FF. A maximum flat region of the efficiency is clearly to be seen and the fact that this maximum extends over a region of 120–200 nm of bl-TiO_2 layer, is therefore convenient for the preparation of large area solar cells in which a fluctuation of bl-TiO_2 layer thickness can be tolerated.

4. Conclusions

Summarizing, to obtain the best overall performance, the bl-TiO_2 layer thickness should lie in the region 120–200 nm. In our lab, we choose the thickness to be 150 nm, which corresponds to 10 spraying cycles. For this thickness, the current flow through the bl-TiO_2 layer is only about 0.01 mA/cm^2 as measured in Schottky diodes at a bias of 400 mV.

Thus, the preparation steps of solid state dye-sensitized nanocrystalline TiO_2 solar cells are optimized with respect to the blocking TiO_2 layer which is one of the important layers in such a multi-layer solar cell. The blocking layer morphology and thickness were characterized using SEM and spectroscopic ellipsometry. The rectifying behavior of compact TiO_2 layers with increasing thickness were studied. An optimum thickness of about 150 nm of compact TiO_2 layer was found to give the best results in terms of rectifying behavior and photovoltaic properties. The automated procedure of preparing the blocking layer guarantees reproducibility in constant thickness and the nature of this crucial layer as seen in the current–voltage characteristics of the solar cells. A standard cell without this blocking layer gives only a few micro-amperes compared to those with blocking layer which give some milli-amperes. Further optimization of this type of solar cell with respect to dye/HTL interface is the current topic of our research and the results will be published later.

Acknowledgements

We thank Sony International (Europe) GmbH, Stuttgart and Sonderforschungsbereich 481 (Project B4) for financial support. The assistance of Mrs. Helga Wietasch (MC I) for the synthesis and of Mrs. Clarissa Abetz (BIMF) for the SEM measurements is kindly acknowledged.

References

[1] B. O'Regan, M. Grätzel, Nature 353 (1991) 737.
[2] (a) K. Tennakone, G.R.R.A. Kumara, I.R.M. Kottegoda, V.P.S. Perera, Chem. Commun. 16 (1999) 15;
(b) K. Tennakone, G.R.R.A. Kumara, A.R. Kumarasighe, K.G.U. Wijayantha, P.M. Sirimanne, Semicond. Sci. Technol. 10 (1995) 1689.
[3] A. Hinsch, J.M. Kroon, R. Kern, I. Uhlendorf, J. Holzbock, A. Meyer, J. Ferber, Prog. Photovolt.: Res. Appl. 9 (2001) 425.
[4] Z.S. Wang, C.H. Huang, Y.Y. Huang, Y.J. Hou, P.H. Xie, B.W. Zhang, H.M. Cheng, Chem. Mater. 13 (2001) 678.
[5] F. Cao, G. Oskam, P.C. Searson, J. Phys. Chem. 99 (1995) 17071.
[6] H. Matsumoto, T. Matsuda, T. Tsuda, R. Hagiwara, Y. Ito, Y. Miyazaki, Chem. Lett. (2001) 26.
[7] N. Papageorgiou, Y. Athanassov, M. Armand, P. Bonhôte, H. Pettersson, A. Azam, M. Grätzel, J. Electrochem. Soc. 143 (1996) 3099.
[8] W. Kubo, K. Murakoshi, T. Kitamura, Y. Wada, K. Hanabusa, H. Shirai, S. Yanagida, Chem. Lett. (1998) 1241.
[9] K. Murakoshi, R. Kogure, Y. Wada, S. Yanagida, Shozo, Chem. Lett. (1997) 471.
[10] C. Jäger, R. Bilke, M. Heim, D. Haarer, H. Karickal, M. Thelakkat, Synth. Met. 121 (2001) 1543.
[11] J. Hagen, W. Schaffrath, P. Otschik, R. Fink, A. Bacher, H.-W. Schmidt, D. Haarer, Synth. Met. 89 (1997) 215.
[12] M. Thelakkat, J. Hagen, D. Haarer, H.-W. Schmidt, Synth. Met. 102 (1999) 1125.
[13] U. Bach, D. Lupo, P. Comte, J.E. Moser, F. Weissörtel, J. Salbeck, H. Spreiter, M. Grätzel, Nature 395 (1998) 583.
[14] J. Krüger, R. Plass, L. Cevey, M. Piccirelli, M. Grätzel, Appl. Phys. Lett. 79 (2001) 2085.
[15] U. Bach, Ph.D. Thesis, EPFL, Lausanne, 2000.
[16] H.K. Pulker, G. Paesold, E. Ritter, Appl. Opt. 15 (1976) 2986.
[17] R. van de Krol, A. Goossens, J. Schoonman, J. Electrochem. Soc. 144 (1977) 1723.
[18] H. K. Pulker, U.S. Patent 3927228 (1975).
[19] M. Thelakkat, C. Schmitz, H.-W. Schmidt, Adv. Mater. 14 (2002) 577.
[20] K.L. Hardee, A.J. Bard, J. Electrochem. Soc. 122 (1975) 739;
K.L. Hardee, A.J. Bard, J. Electrochem. Soc. 124 (1977) 215.
[21] F. Möller, H.J. Tolle, R. Memming, J. Electrochem. Soc. 121 (1974) 1160.
[22] L. Kavan, M. Grätzel, Electrochim. Acta 40 (1995) 643.
[23] M. Okuya, K. Nakade, S. Kaneko, Solar Energy Mater. Solar Cells 70 (2002) 425.
[24] D. Gebeyehu, C.J. Brabec, N.S. Sariciftci, D. Vangeneugden, R. Kiebooms, D. Vanderzande, F. Kienberger, H. Schindler, Synth. Met. 125 (2002) 279.
[25] F. Weissörtel, Ph.D. Thesis, University of Regensburg, 1996.
[26] M.K. Debe, Prog. Surf. Sci. 24 (1987) 54.
[27] T. Gerfin, M. Grätzel, J. Appl. Phys. 79 (1996) 1722.
[28] M. Thelakkat, R. Fink, P. Pösch, J. Ring, H.-W. Schmidt, Polym. Prepr. 38 (1997) 394.